DOI:
10.1021/acs.nanolett.7b01003

Document Version
Early version, also known as pre-print

Citation for published version (APA):
Minovich, A. E., Peter, M., Bleckmann, F., Becker, M., Linden, S., & Zayats, A. V. (2017). Reflective Metasurfaces for Incoherent Light To Bring Computer Graphics Tricks to Optical Systems. *Nano Letters*, *17*(7), 4189-4193. https://doi.org/10.1021/acs.nanolett.7b01003

Reflective metasurfaces for incoherent light to bring computer graphics tricks to optical systems

Alexander E. Minovich,[*,†,‡,¶] Manuel Peter,[‡] Felix Bleckmann,[‡] Manuel Becker,[§] Stefan Linden,[‡] and Anatoly V. Zayats[†]

[†]*Department of Physics, King's College London, Strand, London WC2R 2LS, UK*

[‡]*Nanophotonics Group, Rheinische Friedrich-Wilhelms-Universität Bonn, Physikalisches Institut, Nussallee 12, 53115 Bonn, Germany*

[¶]*Nonlinear Physics Centre, Research School of Physics and Engineering, The Australian National University, Acton, 2601 ACT, Australia*

[§]*Atomic Force Microscopy Group, Rheinische Friedrich-Wilhelms-Universität Bonn, Physikalisches Institut, Nussallee 12, 53115 Bonn, Germany*

E-mail: alexander.minovich@kcl.ac.uk,min124@physics.anu.edu.au

Abstract

The normal mapping technique is widely used in computer graphics to visualize three-dimensional (3D) objects displayed on a flat screen. Taking advantage of optical properties of metasurfaces, which provide a highly efficient approach for manipulation of incident light wavefront, we have designed a metasurface to implement diffuse reflection and used the concept of normal mapping to control its scattering properties. As a proof of principle, we have fabricated and characterized a flat diffuse metasurface imitating lighting and shading effects of a 3D cube. The 3D image is displayed directly

on the illuminated metasurface and it is brighter than a standard white paper by up to 2.4 times. The designed structure performs equally well under coherent and incoherent illumination. The normal mapping approach based on metasurfaces can complement traditional optical engineering methods of surface profiling and gradient refractive index engineering in the design of 3D security features, high-performance planar optical diffusers, novel optical elements, and displays.

Keywords

Metasurfaces, 3D effects, optical diffusers, normal mapping

Shading effect is an important aspect of a three-dimensional (3D) visualization which was used long before stereophotography and holography. It is essential for our perception of volume and depth in two-dimensional projections. An incorrect representation of shading in drawings may easily cause a confusion similar to Penrose's "impossible triangle". In order to achieve shading effects in computer graphics, the technique called normal mapping[1] is implemented in ray-tracing algorithms to create 3D-like features on surface textures, such as regular patterns, graininess, bumps, ripples, bevels for letters or numbers, and so forth (Figure 1a). For scattering surfaces, the orientation of the surface normal determines, in general, lighting and shading effects of a planar representation of a 3D object such that the faces which are turned away from the illumination source look darker in a 2D image (Figure 1b). A mathematical description of the normal mapping procedure involves the manipulation of surface normal vectors, which can be achieved with optical metasurfaces via the tailoring of reflection direction.

Metasurfaces are nanostructured metamaterial layers of a subwavelength thickness which introduce phase changes in the incident light wavefront on the subwavelength scales. They open up opportunities for manipulation of light propagation and beaming properties, such as steering, focusing, spectral filtering, enhancement of nonlinearities, and holographic-type

information encoding among others.[2–4] A strong chromatic aberration has been a serious drawback of the majority of metasurface structures limiting their application in imaging systems (optical lenses) but this problem is gradually being resolved through the implementation of all-dielectric designs.[5–8]

In the presence of a metasurface with a linear phase gradient, the reflection of an electromagnetic wave is described by the generalized Snell's law.[9] In this case, the angle of reflection may differ from the angle of incidence (Figure 1c). In paraxial approximation (small incident angles), it can be shown (see Supporting Information) that the light reflects from such a metasurface (marked S in Figure 1c) as if it would bounce off a virtual interface S' with the orientation of the surface normal $\vec{n}'$ determined by $\theta_{n'} = \frac{1}{2k}\frac{d\Phi}{dx}$, where $\theta_{n'}$ is the angle measured from the actual surface normal vector $\vec{n}$, k is the wavenumber, and $\frac{d\Phi}{dx}$ is the phase gradient induced by the metasurface. This relation shows that in every point of the surface the direction of $\vec{n}'$ can be determined solely by the metasurface properties and independently of the angle of incidence (though at large angles it starts depending on it). Thus, by designing a metasurface phase distribution, one can directly define a spatial map of surface normals, which is equivalent to the effective surface curvature for incident light. In this situation, the interaction of light with the metasurface can be made, to a great degree, independent of interfaceŠs geometric properties. For example, an interface with a concave curvature can be transformed into optically convex or flat surfaces (as seen by incident light) and *vice versa* by designing appropriate properties of a metasurface. A special case of this effect, a metasurface carpet cloak, has been introduced recently: the device corrects the wavefront of a beam reflected from an arbitrary-shaped interface by turning it effectively into a plane wave thus making the surface features optically undetectable.[10–14] For similar applications, metasurface-based diffusers were developed employing random-phase patterns.[15]

All the effects considered in the previous paragraph rely on specular reflection from metasurfaces, when the light coming from a particular direction is reflected in a unique outgoing direction. In order to achieve the described above normal mapping and shading effects, a

metasurface design is needed to manipulate a diffuse scattering. Here, we develop a metasurface that can control the diffuse reflection and show how it can be used to achieve visual representation of 3D objects via the normal mapping method. We experimentally demonstrate this approach on the example of visualization of a cube and discuss the applications of this concept in the design of a wide range of 3D effects.

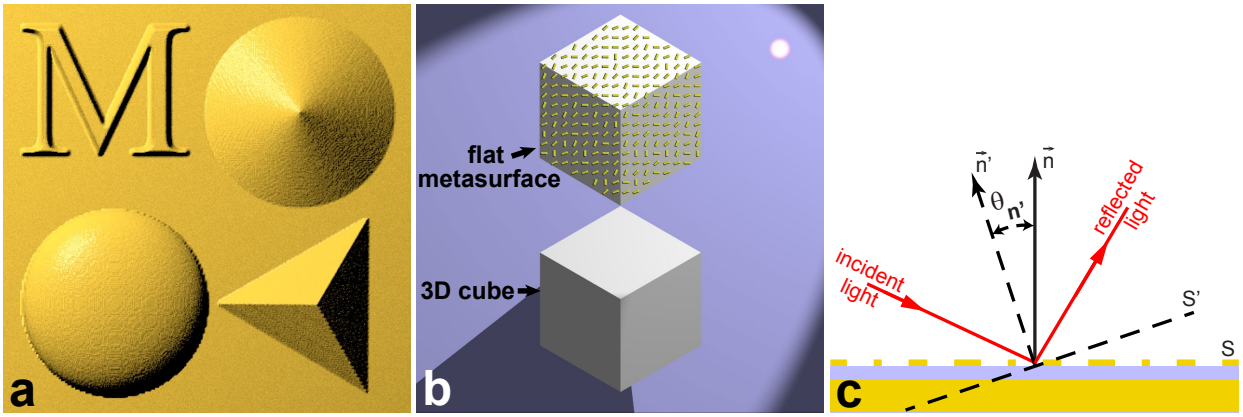

Figure 1: (a) Example of normal mapping implementation in computer graphics: a geometrically flat surface with an overlaying normal pattern corresponding to the letter "M", a cone, a sphere, and a tetrahedron. This is solely the normal map that induces the visible shading effects in this case. In addition, small random normal perturbations (bumps) are introduced to create a grainy, stonelike finish. (b) Illustration of a flat metasurface (top) to imitate shading and lighting effects of a 3D cube through the normal mapping and an actual 3D cube (bottom). Light source location is marked by a small bright ball. (c) Schematic illustration of reflection from a metasurface with a linear phase gradient.

In computer graphics, a default model for a scattering surface is a Lambertian diffuser. Its surface luminance (brightness) appears the same from any point of observation. Thus, the surface brightness is determined only by the effective luminous flux incident on the interface, which is proportional to the cosine of the angle between the normal to a surface and the direction to the illumination source. To realize the normal mapping approach in computer graphics, a 3D object is approximated first by a coarse polygon mesh. Fine geometric surface features are neglected during this stage of meshing. Instead they are encoded into the spatial distribution of surface normal directions (the normal map), which is then overlaid onto the meshed interface to define shading effects produced by the small 3D features (see details in Supporting Information). In this way, the brightness of different parts of the object varies

according to the normal map, providing shading that corresponds directly to the 3D features.

In order to translate the above computer graphics approach to optical domain, a metasurface is needed with the phase variations corresponding to a normal map of a 3D object to be visualized. We have designed such a metasurface with a pattern imitating the shading of a 3D cube to be observed in the direction close to a normal to sampleŠs interface (Figure 1b). The structure is designed in such a way that the cube faces of the image formed by the metasurface appear darker when they are turned away from the light source, mimicking a real 3D shape. When the illumination direction changes, the brightness of the faces of the metasurface-projected cube should vary accordingly as it would for a real 3D cube.

The metasurface-generated phase distribution required to achieve the 3D shading effect should consist of two parts (Figure 2a): a linear phase gradient defining the direction of reflection maximum for the cube faces and a pattern determining diffuse scattering that can be provided by a parabolic phase distribution, mimicking commercial diffusers where microlenses are used (see Supporting Information for details). The linear part is specified separately for each of the cube faces. It is designed to reflect toward the observer (perpendicular to the sample surface) the light incident from the direction of a normal vector of the respective cube face. The parabolic part introduces a diffuse component that expands the angular range of the lighting effect and defines how the cube faces change their brightness with the variation of the angle of incidence, that is, when the light source moves or the metasurface rotates. The smooth variation of the shading of cube faces is provided by the wide angular distribution of the diffuse reflection, which is crucial for the realization of this 3D effect. The angular spectrum (and, therefore, the shading) is determined by the radius of curvature r and truncation diameter D of the small circular areas (patches) where both parabolic and linear phase components are combined (Figure 2b). The summation of a linear and parabolic functions results in a parabola with a shifted origin (a translated parabola), which is shown in Figure 2a (black curve) for 1D case and in Figure 2b for 2D. The patches work similar to microlenses in laser-written diffusers.[16,17] The patches are positioned ran-

domly (Figure 2c–d) to avoid discrete diffraction pattern possible for a regular arrangement (see Supporting Information for details of the design).

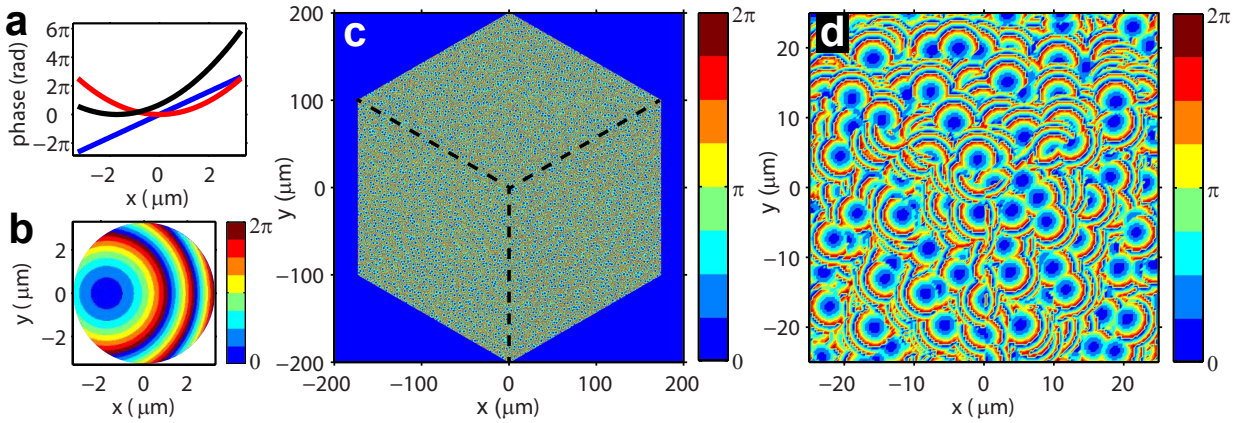

Figure 2: (a) Design of the phase distribution within a microscopic circular patch required for normal mapping and diffuse scattering implementation. Parabolic phase variation (red curve), responsible for diffuse scattering, is combined with a linear phase variation (blue curve) to obtain the required phase dependence (black curve). (b) Calculated phase distribution obtained according to the procedure in (a) across a circular patch. Full span of the phase variation from 0 to 2π is discretized into 8 levels. (c) Phase pattern that consists of multiple circular patches as in (b) is combined using a procedure described in Supporting Information and embedded into the metasurface to imitate a 3D cube (sample 1 with $D = 6.9\,\mu$m and r is randomly distributed in the range $r = 10 - 11\,\mu$m). Dashed lines are the guides for an eye separating different faces of the "cube". (d) Magnified central part of the phase pattern around the cube vertex.

o implement the required phase pattern, we chose a reflective metasurface design based on the Pancharatnam-Berry principle suggested in ref 18. The phase controlling elements are gold nanorods placed above a gold film and separated from it by a dielectric spacer (Figure 3). The structure is illuminated with a circularly polarized light and the observation is performed in the cross-polarization mode. Phase difference introduced in the reflected wave by different nanorods is equal to the double angle of the relative nanorod orientation. The phase modulation is wavelength independent and the structure has a high ($> 80\%$ in theory) efficiency in a broad spectral range $700 - 1100$ nm. In addition, it works in a wide range of angles of incidence (see Supporting Information). All these factors define our choice of the metasurface design. We note that it is possible to achieve similar effects with linearly polarized illumination utilizing gap-plasmon metasurfaces suggested in refs 19 and 20.

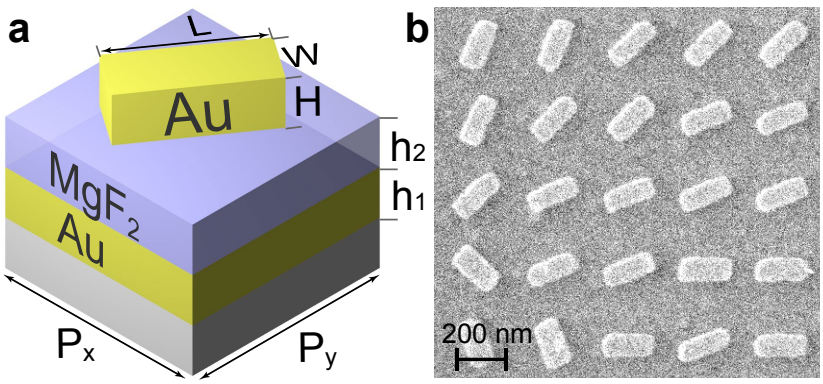

Figure 3: (a) Schematic illustration of a metasurface unit cell ($h_1 = 180$ nm is the gold film thickness, $h_2 = 105$ nm is the MgF_2 spacer thickness, $P_x = P_y = 300$ nm are the unit cell sizes in $x-$ and $y-$directions, respectively, $L = 200$ nm, $W = 80$ nm, and $H = 30$ nm are the gold nanorod length, width, and height, respectively. (b) SEM image of the fabricated metasurface.

The images formed with the metasurface sample 1 ($r = 10 - 11\,\mu$m, $D = 6.9\,\mu$m) are shown in Figure 4 for eight different rotation angles φ_i corresponding to the views of a 3D cube illuminated from different sides. As one can see, the metasurface behaves as a real 3D object when during rotation the cube faces which point toward the light source become brighter. The performance of sample 1 can be observed in a greater detail (with 10° rotation steps) in Movie S1 for coherent illumination. The diameter of round phase patches D controls the scattering properties of the metasurface (smaller D results in narrower angles of diffuse scattering). Sample 2 ($r = 10 - 11\,\mu$m, $D = 3.3\,\mu$m) was designed to achieve the cube faces fading faster as they are being turned away from the source, that is, mainly one of them is visible at a time (Movie S2 and Figure S9 in Supporting Information).

The metasurface pattern works under both coherent and incoherent illumination. This can be understood considering the spatial coherence of light determined by the size and the distance to the light source, according to the van CittertŰZernike theorem.[21] For example, for ceiling spotlights and light bulbs, the coherence area calculated from the theorem has a diameter in the order of 10 μm (see Supporting Information for details). The round phase patches have diameters of 6.9 μm (sample 1) and 3.3 μm (sample 2) and perfectly fit into the estimated coherence area. Therefore, each of the individual patches performs as designed

in terms of steering and diffusing the reflected incoherent light. The interference between distant patches is absent due to the limited spatial coherence area, which is beneficial because it further smooths the angular spectrum for incoherent illumination.

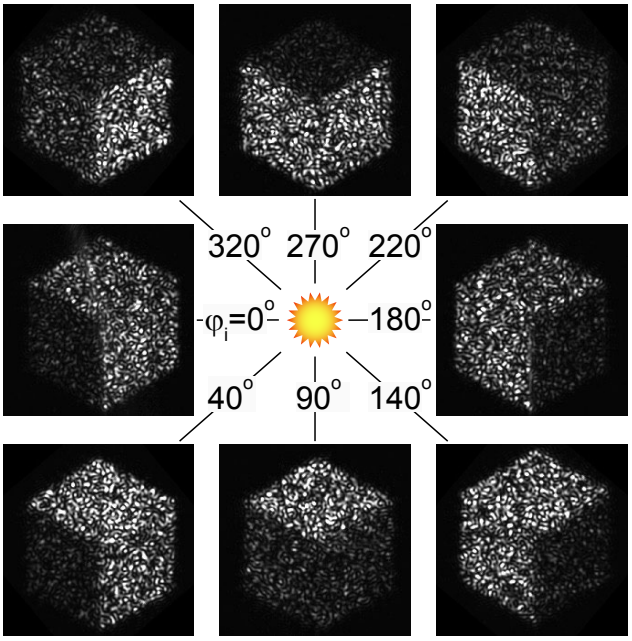

Figure 4: Image of a cube (sample 1) observed at a normal to the metasurface pattern as the light source rotates about the sample (equivalent to the metasurface rotating about the light source). The rotation angle φ_i is indicated for each image. The metasurface is illuminated at an angle of incidence $\theta_i = 21°$ with coherent light of a wavelength of 785 nm. Metasurface parameters: r is randomly distributed in the range $r = 10-11\,\mu$m and a truncation diameter $D = 6.9\,\mu$m. (Snapshots from Movie S1.)

The images obtained with incoherent broadband illumination (720–760 nm) also demonstrate an excellent performance in 3D visualization (Movie S3 and Figure S10 in Supporting Information). No significant differences in graininess of the image were observed with coherent and incoherent illumination. Therefore, the role of speckle formation, typical for diffuse surfaces under coherent illumination, appears to be minimal for the metasurfaces studied. Good performance of the metasurfaces with incoherent light evidences that the 3D effects based on normal mapping can work with incoherent light sources without the need of laser illumination.

Grainy appearance of the structures under both coherent and incoherent illumination is typical for a diffuse surface observed under large magnification (we underline that the metasurface size is just $400 \times 400\,\mu$m limited by fabrication in this proof-of-principle study). The graininess is related to the fact that different parts of the pattern send light in different directions (Movie S4). This sort of graininess can be improved through the optimization of the filling scheme for the circular patches to reduce their overlap, thus eliminating additional phase jumps and image noise associated with it (see Supporting Information). Nevertheless, even in the current design, the image quality can be improved using smaller magnification for observation of the structures (Figure 5). The cube images look rather homogeneous at this low ($40\times$) magnification. The structures are illuminated by an unpolarized, incoherent white-light source (coherence area diameter of approximately $8\,\mu$m) and the reflection is filtered by a standard passive 3D cinema glasses (acting as an output circular polarizing filter). It validates that the developed metasurface does not require any special expensive equipment (lasers, polarizers, phase retarders) to observe 3D image effects and therefore it should make it easier to utilize the structures in practical applications.

To evaluate the scattering efficiency of the metasurfaces, we compared their luminance (brightness) at its maximum (illumination angle about 20°) against a good diffuse surface, white office paper. Under white incoherent illumination, sample 1 shows approximately 0.7 luminance of the white paper, while sample 2 is about 2.4 times brighter than the white paper (the evaluation was limited to the red channel of a CMOS camera because the metasurface working spectral range is limited to > 600 nm, see Figure S6b and Supporting Information). These observations show that the metasurface structures have high enough efficiency to be observed by the naked eye under room illumination.

In summary, we have developed the concept of surface normal mapping for the visualization of 3D objects and shading effects with optical metasurfaces. In order to achieve this, we have designed a metasurface that provides control of diffuse scattering. We have experimentally demonstrated the metasurface-based normal mapping for diffuse surfaces on the

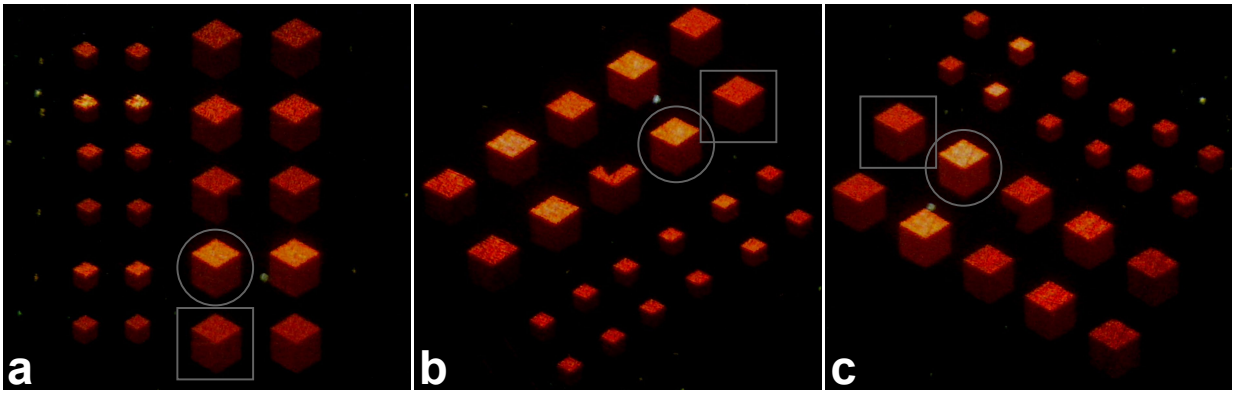

Figure 5: Images of different metasurface patterns under incoherent white-light illumination with a coherence diameter of approximately 8 μm observed at 40× magnification. The rotation angles of the sample φ_i are 0° (a), 120° (b), and 240° (c). The structures are illuminated from the top at the angle of incidence $\approx 35°$. Samples 1 and 2 are marked by a circle and a square, respectively. Other images corresponds to the metasurface patterns with different structure parameters. The only polarizing element used for this observation is a circular polarizing filter from a 3D cinema glasses located before the microscope objective to process reflection. True red color of the images corresponds to the wavelength range of the highest efficiency.

example of 3D shading effects for different angles of illumination. The developed metasurfaces work under broadband incoherent illumination and do not require expensive polarizing elements and lasers: they can be observed with just 3D cinema glasses.

Even though the normal mapping analogy fulfills exactly only for small angles of incidence (paraxial approximation), this fact does not compromise the visual perception of the 3D effect because a human eye does not measure the angles but just tracks the brightness variation of the cube faces. The metasurface-enabled images presented here differ from metasurface-based holograms because the image formation occurs immediately at the metasurface but not in the diffraction field away from the structure. The visual effects based on the surface normal mapping, which we have demonstrated here, can be utilized in security holograms, a special branch of holography, which utilizes reflective relief holograms with such effects as color play, 3D effects, and kinetic images (cartoons), for the protection of brand packages, notes, IDs, credit cards, and so on. It also can be possible to achieve not only static but also dynamically controlled metasurface structures[22] for kinetic 3D images.

The metasurface diffusers we have developed exhibit several advantages (especially at oblique incidence) over scattering surfaces manufactured through the interface profiling. Their flat surface is free from shadows and it minimizes the loss of light in spurious directions due to multiple reflections that may occur when a reflected ray hits a neighbor structure in traditional microlens-based and natural optical diffusers. Thus, we believe that the developed metasurface design can be useful for display technology, metrology, and applications requiring optical systems with engineered scattering (including off-axis geometries). Normal mapping applied to a specular reflecting interface can be used for wavefront shaping either together with or independently from surface profiling. It can enhance or correct surface curvature effects and, therefore, can be employed in optical engineering, in addition to geometric optics and GRIN methods, for designing novel optical elements.

Acknowledgement

We gratefully acknowledge partial financial support from the Erasmus Mundus NANOPHI program. A.M. has been supported by the Newton International Fellowship (The Royal Society). A.Z. acknowledges support from the Royal Society and the Wolfson Foundation.

Supporting Information Available

The following files are available free of charge

Supplementary Text, Materials and Methods

Figs. S1 to S10, Full Reference List

Movies S1 to S4

`http://pubs.acs.org/doi/suppl/10.1021/acs.nanolett.7b01003`.

- Metasurf_SI.pdf: Supporting Information
- S1.avi: sample 1 rotation, laser source.

- S2.avi: sample 2 rotation, laser source.
- S3.avi: sample 1 rotation, incoherent source.
- S4.avi: sample 1 oblique illumination, laser source.

References

(1) Ganovelli, F.; Corsini, M.; Pattanaik, S.; Di Benedetto, M. *Introduction to Computer Graphics: A Practical Learning Approach*; CRC Press, 2015; p 422.

(2) Kildishev, A. V.; Boltasseva, A.; Shalaev, V. M. *Science* **2013**, *339*, 1232009.

(3) Yu, N.; Capasso, F. *Nature Mat.* **2014**, *13*, 139–150.

(4) Minovich, A. E.; Miroshnichenko, A. E.; Bykov, A. Y.; Murzina, T. V.; Neshev, D. N.; Kivshar, Y. S. *Laser & Photonics Reviews* **2015**, *9*, 195–213.

(5) Aieta, F.; Kats, M. A.; Genevet, P.; Capasso, F. *Science* **2015**, *347*, 1342–1345.

(6) Wang, P.; Mohammad, N.; Menon, R. *Scientific Reports* **2016**, *6*, 21545.

(7) Devlin, R. C.; Khorasaninejad, M.; Chen, W. T.; Oh, J.; Capasso, F. *Proceedings of the National Academy of Sciences* **2016**, *113*, 10473–10478.

(8) Khorasaninejad, M.; Shi, Z.; Zhu, A. Y.; Chen, W. T.; Sanjeev, V.; Zaidi, A.; Capasso, F. *Nano Letters* **2017**, *17*, 1819–1824.

(9) Yu, N.; Genevet, P.; Kats, M. A.; Aieta, F.; Tetienne, J.-P.; Capasso, F.; Gaburro, Z. *Science* **2011**, *334*, 333–337.

(10) Ni, X.; Wong, Z. J.; Mrejen, M.; Wang, Y.; Zhang, X. *Science* **2015**, *349*, 1310–1314.

(11) Hsu, L. Y.; Lepetit, T.; Kanté, B. *Progress In Electromagnetics Research* **2015**, *152*, 33–40.

(12) Estakhri, N. M.; Alù, A. *IEEE Antennas and Wireless Propagation Letters* **2014**, *13*, 1775–1778.

(13) Yang, Y.; Wang, H.; Yu, F.; Xu, Z.; Chen, H. *Scientific Reports* **2016**, *6*, 20219.

(14) Orazbayev, B.; Mohammadi Estakhri, N.; Beruete, M.; Alù, A. *Phys. Rev. B* **2015**, *91*, 195444.

(15) Pors, A.; Ding, F.; Chen, Y.; Radko, I. P.; Bozhevolnyi, S. I. *Scientific Reports* **2016**, *6*, 28448.

(16) Morris, G. M.; Sales, T. R. M. Structured screens for controlled spread of light. US Patent No 7033736, 2001.

(17) Sales, T. R. M.; Schertler, D. J.; Chakmakjian, S. *Proc. SPIE* **2006**, *6290*, 629005–10.

(18) Zheng, G.; Mühlenbernd, H.; Kenney, M.; Li, G.; Zentgraf, T.; Zhang, S. *Nature Nanotechnology* **2015**, *10*, 308–312.

(19) Pors, A.; Bozhevolnyi, S. I. *Opt. Express* **2013**, *21*, 27438–27451.

(20) Pors, A.; Nielsen, M. G.; Bozhevolnyi, S. I. *Nano Letters* **2015**, *15*, 791–797.

(21) Born, M.; Wolf, E. *Principles of optics*; Cambridge University Press, Cambridge, 2005; p 572.

(22) Bar-David, J.; Stern, L.; Levy, U. *Nano Letters* **2017**, *17*, 1127–1131.